Estimation of Atlantic Water transit times in East Greenland fjords using a ^{233}U-^{236}U tracer approach

Lin, Gang; Lin, Mu; Qiao, Jixin; Sejr, Mikael K.; Steier, Peter; Meire, Lorenz; Stedmon, Colin A.

Published in:
Chemical Geology

Link to article, DOI:
10.1016/j.chemgeo.2022.121007

Publication date:
2022

Document Version
Publisher's PDF, also known as Version of record

Chemical Geology 607 (2022) 121007

Contents lists available at ScienceDirect

Chemical Geology

journal homepage: www.elsevier.com/locate/chemgeo

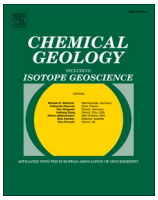

Estimation of Atlantic Water transit times in East Greenland fjords using a ^{233}U-^{236}U tracer approach

Gang Lin [a], Mu Lin [a], Jixin Qiao [a,*], Mikael K. Sejr [b,c], Peter Steier [d], Lorenz Meire [e,f], Colin A. Stedmon [g]

[a] Department of Environmental and Resource Engineering, Technical University of Denmark, DK-4000 Roskilde, Denmark
[b] Department of Bioscience, Aarhus University, Vejlsøvej 25, 8600 Silkeborg, Denmark
[c] Arctic Research Centre, Aarhus University, Aarhus, Denmark
[d] VERA Laboratory, Faculty of Physics, Isotope Physics, University of Vienna, Währinger Straße 17, A-1090 Vienna, Austria
[e] Greenland Climate Research Centre, Greenland Institute of Natural Resources, Kivioq 2, P.O. Box 570, 3900 Nuuk, Greenland
[f] Department of Estuarine and Delta Systems, Royal Netherlands Institute of Sea Research, Yerseke, Netherlands
[g] National Institute of Aquatic Resources, Technical University of Denmark, Kemitorvet, 2800 Kgs. Lyngby, Denmark

ARTICLE INFO

Editor: Don Porcelli

Keywords:
^{233}U
^{236}U
Nutrients
East Greenland fjords
Atlantic Water transit time
Arctic Ocean

ABSTRACT

Water mass composition and transit times of outflowing waters from the Arctic Ocean can reflect changes of polar climate and ocean circulation upstream. In this study we apply a novel approach using anthropogenic uranium tracers (^{233}U and ^{236}U), combined with salinity, and nutrients (nitrate and phosphate) to estimate transit times of waters from the Atlantic passing through the Arctic and into East Greenland fjords. In Polar Surface Water (PSW, typically found in surface ~150 m of the fjords) the dominant source of ^{236}U is European reprocessing plants (63%) while in Arctic Atlantic Water (AAW, typically directly below PSW in these fjords) it is much less (26%) and the ^{236}U signal is dominated by the global fallout contribution. Here we isolate the ^{236}U signal from reprocessing plants using $^{236}U/^{233}U$ ratios and use the temporal development in ^{236}U discharges to estimate transit times for Atlantic Water entering the Arctic Ocean and exiting as either PSW or AAW on the Greenland Shelf. PSW, which flows into the fjords from the shelf, has a transit time of between 6 and 14 years from the Arctic entrance (Barents Sea Opening, 74°N, 19°E). The transit time of AAW, which is entrained into upwelling subglacial discharge in the inner parts of the fjords, is in the order of 24–25 years since entrance in the Barents Sea. The findings indicate the potential of this novel ^{233}U-^{236}U approach to trace Atlantic Water circulation in the Arctic Ocean. The method offers independent transit time estimates to compare with circulation models and indicates the potential time lag between documented recent change in properties of water leaving the Arctic Ocean and the upstream processes contributing to these changes.

1. Introduction

Changes in the supply and distribution of heat and freshwater in the Arctic Ocean can potentially influence global ocean circulation and climate (Aagaard and Carmack, 1989; Rahmstorf, 2002; Tsubouchi et al., 2021; Wang, 2021). Inflowing waters from the Atlantic and Pacific bring heat to the Arctic Ocean and result in loss of sea ice (Beszczynska-Möller et al., 2011; Polyakov et al., 2017; Skagseth et al., 2020). As Pacific Water is less saline than Atlantic Water, it contributes together with precipitation and river discharge, as a source of freshwater (Serreze et al., 2006). These freshwater contributions serve to maintain a density stratification in the Arctic Ocean, and also supply freshwater to the North Atlantic via the Canadian Archipelago and the East Greenland Shelf. Here the freshwater supply can potentially influence Atlantic meridional overturning circulation (Rahmstorf, 2002; Ionita et al., 2016). Atlantic, Pacific and fresh waters are integrated into Polar Surface Water (PSW) with sub-zero temperature and variable salinity that are transported by the outflowing East Greenland Current. The fjords of Northeast Greenland often have a layer of PSW lying above warmer Arctic Atlantic Water (AAW, more saline and with temperatures above 0 °C) which represents Atlantic Water that has entered the Arctic Ocean and recirculated out. AAW is located at intermediate depths (~300–800 m) in the Arctic Ocean below PSW (Rudels et al., 2004). Warmer AAW (0–2 °C) carries more heat which facilitates the melt of sea ice (Polyakov

* Corresponding author.
E-mail address: jiqi@dtu.dk (J. Qiao).

https://doi.org/10.1016/j.chemgeo.2022.121007
Received 6 March 2022; Received in revised form 6 June 2022; Accepted 26 June 2022
Available online 30 June 2022

et al., 2017). Measurements of surface and subsurface waters of these fjords can reflect the changing properties of PSW and AAW exiting the Arctic Ocean and transported along the East Greenland Shelf (Sejr et al., 2017). These properties are currently changing in response to changes occurring upstream in the Arctic Ocean. The clearest trends are from 2000 onwards. PSW entering the fjords from the shelf and has freshened (Sejr et al., 2017) and the thickness of the PSW layer has thinned (Gjelstrup et al., 2022). There is also a greater presence of AAW, particularly evident as warmer bottom water temperatures on the shelf and in fjords (Schaffer et al., 2017, 2020; Gjelstrup et al., 2022). The transport of Atlantic Water in PSW and AAW plays a significant role in the Arctic climate and environment, so a good tracer approach is necessary for investigating and estimating its circulation pattern and transit time to explain the hydrographic and biogeochemical processes.

Significant amounts of radioisotopes have been discharged to the North Atlantic Ocean from the two European reprocessing plants (RP) at Sellafield (SF, United Kingdom) and La Hague (LH, France). This imparts a signature on Atlantic Water as it moves northwards toward the Arctic (Fig. 1). Discharges of several radioisotopes from the two plants have varied over the last 50 years, and this presents an opportunity to use these radioisotopes as transient tracers to resolve circulation patterns and timescales (Smith et al., 2011; Christl et al., 2012; Christl et al., 2015; Casacuberta et al., 2018; Wefing et al., 2019; Wefing et al., 2021). In the North Atlantic and Arctic Oceans, ^{129}I-^{236}U tracer pair has been used to trace the path of three branches of Atlantic Water (Casacuberta et al., 2018). Wefing et al. (2019 and 2021) estimated the transit times of

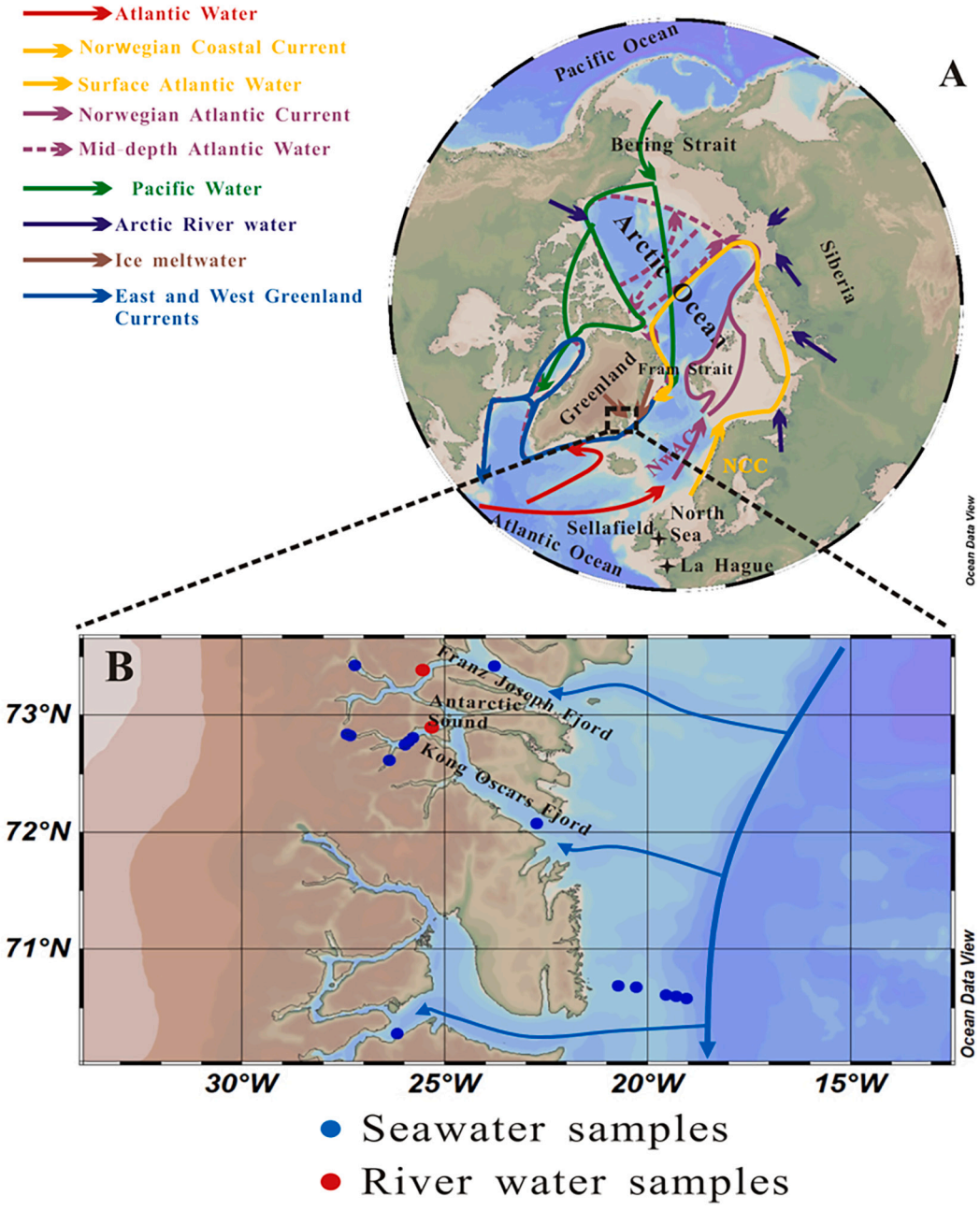

Fig. 1. Simplified depiction of general circulation pattern in the North Atlantic and Arctic Ocean (A), location of sampling sites (B). Currents and water masses in the Arctic Ocean are Norwegian Coastal Current (NCC; orange), Norwegian Atlantic Current (NwAC; purple), Pacific Water (green), Arctic rivers water (dark blue), ice meltwater (brown) and East and West Greenland Current (mixture of Atlantic Water, Pacific Water, Arctic rivers water and ice meltwater, blue). Solid arrows are surface water, and dotted arrows are deeper water. Black crosses mark two main European reprocessing plants at Sellafield and La Hague. (For interpretation of the references to colour in this figure legend, the reader is referred to the web version of this article.)

Atlantic Water in the Arctic Ocean and the Fram Strait using a binary mixing model with $^{129}I/^{236}U$ ratios and ^{236}U concentrations as signatures. The transit times of Atlantic Water in PSW from the entrance of the Arctic Ocean (74°N, 19°E) to the Amundsen Basin and the western Fram Strait were reported to be 9–16 years and 12–17 years respectively (Wefing et al., 2021). The corresponding transit time for Atlantic Water in AAW was estimated to be 16–23 years (Wefing et al., 2019).

While this approach offers estimates of transport times to compare with models of ocean circulation, it assumes that the two elements (I and U) have the same physiochemical behaviors in seawater and that $^{129}I/^{236}U$ ratios are not altered by processes other than mixing along the transport pathways. However, iodine and uranium have different biogeochemical properties in seawater (Tsungogai and Henmi, 1971; Klimkhammer and Palmer, 1991; Rutgers van der Loeff and Geibert, 2008). Iodine is readily enriched in waters containing high content of organic matter (Schwehr et al., 2005), while uranium behaves non-conservatively in anoxic waters (Dunk et al., 2002; Lin et al., 2021a; Andersson et al., 1995). In open areas of the Arctic Ocean, both iodine and uranium may behave conservatively. Whereas in estuarine environments, such as the Siberian coast, contribution of organic matter from Siberian rivers may alter the behavior of iodine and uranium to be non-conservative at different extents, thus changing $^{129}I/^{236}U$ ratios.

In addition, the current oceanic tracer studies using ^{236}U suffer from methodological difficulties to distinguish different ^{236}U sources. Besides the natural inventory of 35 kg ^{236}U in the Earth's crust (Steier et al., 2008), the dominating sources of anthropogenic ^{236}U in the environment are the global fallout (GF) from atmospheric nuclear weapons testing since 1950s (900–1400 kg in total) and the discharges from SF (237 ± 21 kg) and LH (46 kg) which were primarily released into the North Atlantic Ocean (Steier et al., 2008; Sakaguchi et al., 2009; Castrillejo et al., 2020).

RP signal that is discharged into the northeastern North Atlantic Ocean tags Atlantic Water thus makes it easily identifiable. A previous study indicated that radioactive releases from SF were transported by Scottish Coastal Current from the Irish Sea to the northern Scotland coast and the North Sea (Christl et al., 2017). A branch of Scottish Coastal Current carrying SF signal enters the North Sea and mixes with the releases from LH transported by the English Channel Current. SF and LH signals are partly merged in the North Sea, transported northward by the Norwegian Coastal Current (NCC) to the Barents Sea, and subsequently advected to the surface and subsurface layer of the Arctic Ocean to form PSW (Wefing et al., 2021). The branches of Scottish Coastal Current (SF) and English Channel Current (LH) also join the Norwegian Atlantic Current (NwAC), and further enter the intermediate layer of the Arctic Ocean forming AAW (Wefing et al., 2021).

The ubiquitous ^{236}U contributions from GF inevitably introduce uncertainties in transit time estimates for Atlantic Water in the Arctic Ocean, especially in the coastal regions of the Arctic fjords which may receive more GF input from the terrestrial areas via glaciers melt and river runoff. The uranium isotope signature in glacial meltwater likely varies from pre-post nuclear weapons testing to present due to the changing GF contribution. It can therefore be beneficial to isolate the RP-derived ^{236}U rather than assume a constant value for GF-derived ^{236}U. This can be achieved by applying a uranium dual tracer (^{233}U-^{236}U) approach.

In contrast to ^{236}U, almost all ^{233}U is supplied by GF (Hain et al., 2020), which results in large difference in $^{236}U/^{233}U$ atomic ratios between GF (71.4 ± 7.7) and RP (LH, 1–10 × 10^6) (Hain et al., 2020; HELCOM MORS Discharge database [WWW Document], 2020; Qiao et al., 2020). $^{236}U/^{233}U$ ratios can therefore be used to distinguish contributions of ^{236}U from GF and RP, and thereby refine the ^{236}U approach for trace Atlantic Water transit times. Atlantic Water contains both RP and GF derived ^{236}U whereas other waters only contain a GF-derived ^{236}U signal. The time-dependent variation of RP-derived ^{236}U in discharge and subsequently also in recipient Atlantic Water can be used to estimate the contribution and transit time of Atlantic Water in the Arctic and subpolar regions. Compared to other radioisotopes, such as ^{90}Sr (half-life 28.8 a) and ^{137}Cs (half-life 30.2 a) (Dahlgaard, 1995), ^{233}U and ^{236}U have superior properties including very long half-lives (^{233}U: 0.159 Ma; ^{236}U: 23.4 Ma) and high solubility in the open ocean (Sakaguchi et al., 2012; Eigl et al., 2013; Casacuberta et al., 2014; Hain et al., 2020). Importantly, being isotopes of the same element, $^{236}U/^{233}U$ ratios are not affected by geochemical processes along the transport (Hain et al., 2020; Qiao et al., 2020). Different from anthropogenic chemical tracers, such as chlorofluorocarbons (CFCs) and sulfur hexafluoride (SF6) (Fine, 2011) which enter the ocean everywhere by air-sea exchange, anthropogenic radioisotope tracers have the advantage of constrained source functions from RP, thus provide reliability in their tracer applications for water mass transport. In the case of ^{233}U-^{236}U, the dominant point-source release of ^{236}U from SF and LH make them suitable to trace large-scale water mass transport in the North Atlantic-Arctic Ocean.

In our previous work, ^{236}U source terms were estimated for the Greenland coast based on ^{233}U and ^{236}U data in the surface seawater (0–10 m), wherein dominating ^{236}U contribution (~ 70%) were found from RP and ~ 30% from GF (Qiao et al., 2020). In this work, we aim to explore the opportunity of using the ^{233}U-^{236}U tracer approach to estimate the transit times of Atlantic Water in the Arctic Ocean. The measurements arise from opportunistic sampling in a Northeast Greenland fjord complex (Fig. 1). Isotope measurements where combined with salinity, nitrate and phosphate measurements to resolve mixing and transit times. We recognize that the study region might not be ideal to prove a new approach for RP-derived radioisotopes as it is quite far downstream from the source of RP. We believe it is still relevant to demonstrate the potential of the proposed ^{233}U-^{236}U tracer approach in oceanic studies.

2. Materials and methods

2.1. Study area and sampling

The study region is located halfway along the East Greenland coast in the Kong Oscars and Franz Josef fjord system (Fig. 1A and B). Sampling was carried out on board the Royal Danish Naval vessel HMDS Lauge Koch in August 2018. Water profiles of salinity and temperature were collected using a SeaBird SBE25 CTD (conductivity, temperature, depth), and water samples were collected using 10-L Niskin bottles.

A total of 26 seawater samples (5–10 L) were collected in the East Greenland coast for uranium isotopes analyses among which 13 were water column samples and 13 were surface water samples (Table S1). Two additional river water samples were taken from the Antarctic Sound in the Kong Oscar fjord complex. Seawater samples were stored in 10-L precleaned plastic bottles after first rinsing with sample water and sent back to the laboratory for ^{233}U, ^{236}U and ^{238}U processing. In addition, seawater samples for nutrient measurement were collected in acid-washed polyethylene bottles and frozen at −20 °C. Ten seawater samples were analyzed through using an autoanalyzer (Skalar) based on the approach of Hansen and Koroleff (1999). The average precision on nitrate and phosphate measurement is 1%. Due to opportunistic sampling for uranium measurement, only 10 samples for nutrient analyses can be matched.

2.2. Determination of ^{233}U, ^{236}U, and ^{238}U

To determine ^{233}U and ^{236}U, an optimized radiochemical procedure was utilized to extract U isotopes from 5 to 10 L seawater samples (See supporting information) (Qiao et al., 2015; Lin et al., 2021b). The accelerator mass spectrometry (AMS) measurement of $^{236}U/^{238}U$ and $^{233}U/^{238}U$ measurement was carried out at the Vienna Environmental Research Accelerator (VERA) facility in the University of Vienna. The detailed setup and method of AMS measurement has been reported elsewhere (Steier et al., 2010; Steier et al., 2019; Hain et al., 2020). Each

sample was measured by AMS for three cycles with counting times of 300–1000 s for ^{236}U and 2000–4500 s for ^{233}U in each cycle, respectively, to obtained average atomic ratios of $^{236}U/^{238}U$ and $^{233}U/^{238}U$. Typically, relative uncertainties of $^{236}U/^{238}U$ and $^{233}U/^{238}U$ ratios obtained in this work were below 10% and 30%, respectively. In case of higher uncertainties obtained, the measured values were deemed as outliers. To obtain ^{233}U and ^{236}U concentrations in seawater samples, ^{238}U concentration in seawater samples were measured using inductively coupled plasma mass spectrometry (ICP-MS) (ICP-QQQ 8800, Agilent) after dilution with 0.5 M HNO_3 (Qiao and Xu, 2018). Indium or bismuth was utilized as the internal standard.

Satisfactory chemical yields for U (60–80%) monitored via ^{238}U were

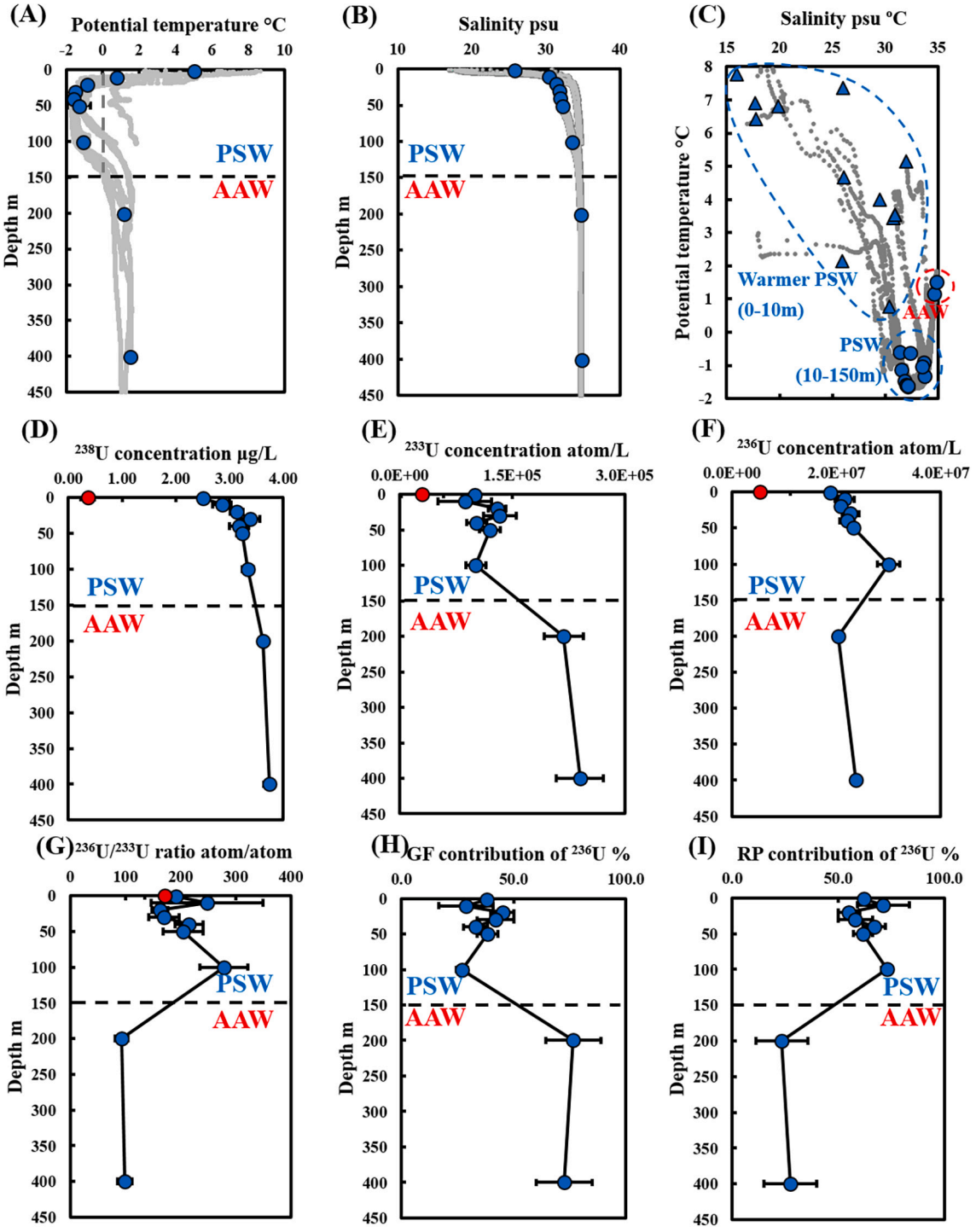

Fig. 2. The depth profiles of different measured and calculated parameters. The profiles are divided into two main layers: Polar Surface Water (PSW, $\theta < 0$ °C) and Arctic Atlantic Water (AAW, $0 < \theta < 2$ °C). The parameters are potential temperature θ (A), salinity (B), the diagram of potential temperature-salinity (C, triangle data at 1–10 m depths, circle dots data at 10–100 m depths), ^{238}U concentration (D), ^{233}U concentration (E), ^{236}U concentration (F), $^{236}U/^{233}U$ atomic ratio (G), global fallout (GF) contribution of ^{236}U (H), reprocessing plants (RP) contribution of ^{236}U (I). All dots present the averaged values with uncertainties for the river (red) and seawater (blue) samples at the same depth. Grey profiles represent the full profiles measured by the in situ sensors. (For interpretation of the references to colour in this figure legend, the reader is referred to the web version of this article.)

achieved for the samples analyzed in this work. The chemical yield of uranium during the chemical separation was estimated as the ratio of ^{238}U mass in the eluate and ^{238}U mass in the original seawater sample. Herein, we assume uranium was quantitatively recovered during the AMS target preparation after the chemical separation, which was verified in our earlier study (Qiao et al., 2015). Blank samples were prepared along with each batch (typically $n = 7$) of samples following the same procedure as for the seawater. To reduce the background levels of ^{233}U and ^{236}U, special measures were implemented, including purification of chemicals, utilization of laminar flow bench, and acid boiling for glassware. Under such well-controlled conditions, the count rates of ^{236}U and ^{233}U in the monitored blank samples were typically <30% of the corresponding samples. The removed contribution from laboratory background and the combined uncertainties of ^{233}U/^{238}U and ^{236}U/^{238}U is calculated based on the law of uncertainty propagation, details are summarized in the supporting information.

3. Results

3.1. Water column properties

Practical salinity (S) and potential temperature (θ) of seawater in the East Greenland fjords ranged from 16.02 to 34.89 psu and from −1.63 °C to 7.78 °C, respectively. As the entire study area once beyond the local impact of marine terminating glaciers showed a common stratified and spatially homogeneous structure (as evident from S and θ profiles shown in Fig. 2). Uranium results in multiple samples collected at the same depth ($n = 13$ at 1 m; $n = 2$ at 20 m; $n = 3$ at 50 and 100 m, respectively) were averaged into one value with a combined uncertainty, except for the single sample at 10, 30, 40, 200 and 400 m, respectively (Fig. 2, Table S1). Down the water column, θ quickly decreased from 7.78 °C to −1.63 °C within 0–50 m depth, and then gradually increased to 1.54 °C at 400 m depth (Fig. 2A). In the depth profile of salinity, there was a steep increase (16.02–30.42) in the upper 10 m depth followed by a gentle increase (30.42–34.89) in the subsurface and deep waters (Fig. 2B). Measurements from stations where no uranium samples were collected are shown in grey and emphasize the lateral homogeneity of the sampled region (Fig. 2A-B).

The East Greenland fjords and their neighboring shelf waters are mainly affected by the East Greenland Current from the Arctic Ocean via the Fram Strait, where the surface (and subsurface) and deeper layer are dominated by PSW and AAW, respectively (Rudels, 2009; Wefing et al., 2019). These waters can be distinguished (Fig. 2C), based on different potential temperature and salinity. Waters sampled here that had a temperature < 0 °C and salinity <34 were defined as PSW. Warmer (0–2 °C) and more saline samples were defined as AAW. At the very surface (upper 10 m) the properties of PSW were influenced by surface warming and entrainment of meltwater (Fig. 2). The radioisotope samples can be segregated into originating from one of the two layers, PSW distributed at 0–150 m and AAW distributed below 150 m depth (Fig. 2).

3.2. Uranium isotopes

^{238}U concentrations in the seawater samples varied between 1.26 and 3.74 μg/L (Fig. 2D, Table S1) and revealed a strong linear correlation with salinity ($R^2 = 0.90$, slope = 0.109, $p < 0.01$). Atomic ratios of ^{236}U/^{238}U (2.22–5.36 × 10^{-9}) and ^{233}U/^{238}U (1.10–2.52 × 10^{-11}) were higher than their expected natural background levels (e.g., 10^{-14}–10^{-13} of ^{236}U/^{238}U in natural seawater and 10^{-13}–10^{-11} of ^{233}U/^{238}U in minerals) (Steier et al., 2008; Hain et al., 2020; Villa-Alfageme et al., 2019), indicating the contribution of anthropogenic U in these waters. ^{233}U concentrations, ranging within 5.90–14.1 × 10^4 atom/L, showed no systematic change with depth in PSW, but were significantly higher (21.6–23.8 × 10^4 atom/L) in AAW (Fig. 2E). ^{236}U concentrations gradually increased from 14.5 ± 0.9 × 10^6 atom/L to 34.9 ± 3.0 × 10^6 atom/L in PSW, but decreased again (20.4–23.6 × 10^6 atom/L) in AAW (Fig. 2F). Relatively higher ^{236}U/^{233}U ratios were observed in PSW (137–344) than those in AAW (94–99), indicating that the upper 100 m of the East Greenland fjords received more RP signals than the deep waters (Fig. 2G). ^{233}U and ^{236}U concentrations in East Greenland river water were (2.53–3.46) × 10^4 atom/L and (3.31–7.33) × 10^6 atom/L, respectively (Fig. 2E and F, Table S1).

3.3. Source terms of ^{236}U

Qiao et al. (2020) developed an approach to distinguish the source terms of ^{236}U in the surface seawater of Greenland coast using atomic ratios of ^{233}U/^{236}U. Here we use the following equations modified from Qiao et al. (2020) to calculate the GF and RP fraction, and GF and RP-derived ^{236}U concentration.

$$P_{GF} = \frac{R_{GF}^{236/233}\left(R_{RP}^{236/233} - R_S^{236/233}\right)}{R_S^{236/233}\left(R_{RP}^{236/233} - R_{GF}^{236/233}\right)} \approx \frac{R_{GF}^{236/233}}{R_S^{236/233}} \quad (1)$$

$$P_{RP} = 1 - P_{GF} \quad (2)$$

$$C_{s,GF}^{236} = C_s^{236} \times P_{GF} = R_{GF}^{236/233} \times C_S^{233} \quad (3)$$

$$C_{s,RP}^{236} = C_s^{236} \times P_{RP} = C_s^{236} - C_{s,GF}^{236} \quad (4)$$

where P_{GF} and P_{RP} are GF and RP fraction in the seawater sample; $R_S^{236/233}$ is the ^{236}U/^{233}U atomic ratio of the seawater sample; $R_{RP}^{236/233}$ is RP endmember with the representative value of 1 × 10^7; $R_{GF}^{236/233}$ is GF endmember with the representative value of 71.4 ± 7.7 (Hain et al., 2020); C_s^{233} is the measured ^{233}U concentration in the seawater sample; and C_s^{236}, C_{GF}^{236}, and C_{RP}^{236} are total, GF-derived and RP-derived ^{236}U concentration in the seawater samples, respectively. We acknowledge that $R_{GF}^{236/233}$ in Atlantic Water might be either different or variable over the last 50 years, thus might introduce additional uncertainties in this endmember algorithm. Nevertheless, as the most intensive deposition of global fallout was in the mid-1960s, it is likely that the distribution of GF ^{236}U and ^{233}U reached nearly steady state in the modern ocean surface (as indicated by other radionuclides from GF as well, such as ^{137}Cs and ^{90}Sr). Therefore, we expect that the uncertainties in the GF endmember in the Atlantic Water should be reasonably low. This is partially supported by the comparable ^{236}U/^{233}U ratios in corals and sediments from the Pacific Ocean since 1970s to the represented GF value (Hain et al., 2020; Qiao et al., 2022). Therefore, in this work, we adopted the uncertainty (11%) as derived from the representative GF ^{236}U/^{233}U ratio (71.4 ± 7.7) without giving additional uncertainty in the calculation.

The combined uncertainties of GF and RP contributions of ^{236}U are estimated through the law of uncertainty propagation (BIPM et al., 2008):

$$\begin{aligned} u(P_{GF}) &= \sqrt{\left(\frac{\partial P_{GF}}{\partial R_{GF}^{236/233}}\right)^2 \times u^2\left(R_{GF}^{236/233}\right) + \left(\frac{\partial P_{GF}}{\partial R_S^{236/233}}\right)^2 \times u^2\left(R_S^{236/233}\right)} \\ &= \sqrt{\left(\frac{1}{R_S^{236/233}}\right)^2 \times u^2\left(R_{GF}^{236/233}\right) + \frac{\left(R_{GF}^{236/233}\right)^2}{\left(R_S^{236/233}\right)^4} \times u^2\left(R_S^{236/233}\right)} \end{aligned} \quad (5)$$

$$u(P_{RP}) = \sqrt{\left(\frac{\partial P_{RP}}{\partial P_{GF}}\right)^2 \times u^2(P_{GF})} = u(P_{GF}) \quad (6)$$

where $u(P_{GF})$ and $u(P_{RP})$ are the combined uncertainties of GF-derived and RP-derived ^{236}U concentrations, respectively; and $u(R_{GF}^{236/233})$ and $u(R_S^{236/233})$ are the uncertainties for the representative ^{236}U/^{233}U ratio of GF (7.7) and the measurement samples.

The relative uncertainties of GF and RP contributions of ^{236}U range from 14 to 42% and 7–51%, respectively. And the average weights for GF contribution of ^{236}U in GF and the seawater sample are 0.33 and 0.67, respectively. In addition, the combined uncertainties of GF-derived and RP-derived ^{236}U concentrations are estimated through the law of uncertainty propagation (BIPM et al., 2008):

$$\mathrm{u}\left(C^{236}_{s,GF}\right) = \sqrt{\left(\frac{\partial C^{236}_{s,GF}}{\partial C^{233}_{s}}\right)^2 \times u^2\left(C^{233}_{s}\right) + \left(\frac{\partial C^{236}_{s,GF}}{\partial R^{236/233}_{GF}}\right)^2 \times u^2\left(R^{236/233}_{GF}\right)} = \sqrt{\left(R^{236/233}_{GF}\right)^2 \times u^2\left(C^{233}_{s}\right) + \left(C^{233}_{S}\right)^2 \times u^2\left(R^{236/233}_{GF}\right)} \quad (7)$$

$$\mathrm{u}\left(C^{236}_{s,RP}\right) = \sqrt{\left(\frac{\partial C^{236}_{s,RP}}{\partial C^{236}_{s}}\right)^2 \times u^2\left(C^{236}_{s}\right) + \left(\frac{\partial C^{236}_{s,RP}}{\partial C^{236}_{s,GF}}\right)^2 \times u^2\left(C^{236}_{s,GF}\right)} = \sqrt{u^2\left(C^{236}_{s}\right) + u^2\left(C^{236}_{s,GF}\right)} \quad (8)$$

where $u(C^{236}_{s,\ GF})$ and $u(C^{236}_{s,\ RP})$ are the combined uncertainties of GF-derived and RP-derived ^{236}U concentrations, respectively; $u(C^{233}_{s})$ and $u(C^{233}_{s})$ are the measurement uncertainties of ^{233}U and ^{236}U concentrations, respectively; and $u(R^{236/233}_{GF})$ is the uncertainty for the representative ^{236}U/^{233}U ratio of GF (7.7).

The relative uncertainties of GF-derived and RP-derived ^{236}U concentrations vary from 15 to 42% and 11–53%, respectively. The average weights for ^{236}U/^{233}U atomic ratio in the seawater sample and GF are 0.68 and 0.32, respectively.

Based on these equations, the proportion of ^{236}U derived from GF and RP in East Greenland fjords can be calculated (Table S1). The GF contributions of ^{236}U in PSW of East Greenland fjords range from 21 ± 6 – 52 ± 8%, with the RP contributions representing the remainder (Fig. 2G and H). Distinct changes in ^{236}U source distribution were observed in AAW: GF contributions of ^{236}U increased by a factor of 2 and became the dominating (72 ± 12 – 76 ± 12%) source, whereas the RP contributions decreased to <30%.

4. Discussion

4.1. ^{233}U and ^{236}U in Polar Surface Water, Arctic Atlantic Water, and freshwater

Notable differences (approximate factor of 2) were observed in the ^{233}U concentration and ^{236}U/^{233}U ratio between PSW and AAW (Fig. 2E and G). In comparison, the variability in ^{236}U concentration down the water columns was much lower. As ^{233}U was mainly deposited in GF in 1950s–1960s (Hain et al., 2020; Lin et al., 2021a), lower ^{233}U concentrations can be expected in the comparatively younger PSW. Salinity measurements indicate that while PSW is less saline (Fig. 2B), even dilution with freshwater devoid of ^{233}U cannot explain the lower concentrations in PSW. The differences in the ratios likely reflect the differences in the source and transport pathways of anthropogenic uranium. Higher ^{236}U/^{233}U ratios in the PSW indicate a greater RP contribution in the upper 100 m due to the dominating supply from the NCC to surface water of the Arctic Ocean. The NCC supplies PSW with a greater RP ^{236}U contribution than that supplied by the NwAC to AAW (Fig. 2I) (Casacuberta et al., 2018; Wefing et al., 2021). In contrast, ^{236}U in AAW is predominantly from GF contribution (ca. 74%) (Fig. 2H) reflecting the older GF-derived signal (primarily deposited in 1960s) (Sakaguchi et al., 2016), which was mostly likely advected into deeper water columns by Atlantic Water tagged with the GF in other locations.

The averaged concentration (with standard deviation) of ^{236}U in the upper 10 m of East Greenland fjords (18.9 ± 3.3 × 10^6 atom/L) is comparable to those reported for the Amundsen Basin (24.7 ± 3.6 × 10^6 atom/L) (Casacuberta et al., 2016), the western Fram Strait (20.8 ± 0.8 × 10^6 atom/L) (Wefing et al., 2019) and East Greenland coastal surface waters (18.8 ± 6.4 × 10^6 atom/L) (Qiao et al., 2020). All these values are higher than the expected if ^{236}U concentrations in the Arctic Ocean solely resulted from GF. This indicates the importance of an additional ^{236}U contribution from RP in Europe. The averaged values of GF-derived ^{236}U (7.0 ± 1.5 × 10^6 atom/L) and RP-derived ^{236}U (11.9 ± 2.6 × 10^6 atom/L) obtained for surface seawater (0–10 m) is comparable to those reported earlier from 2012 to 2016 (GF-derived ^{236}U concentration: 5.5 ± 1.9 × 10^6 atom/L and RP-derived ^{236}U concentration: 13.3 ± 4.5 × 10^6 atom/L) (Qiao et al., 2020).

4.2. Estimation of Atlantic Water transit time

4.2.1. End-member mixing algorithm

Here we attempt to use RP-derived ^{236}U concentration calculated from ^{233}U-^{236}U tracer to estimate the transit time of Atlantic Water in PSW of the East Greenland fjords. As the RP signal is unique and constrained to the Atlantic Water, we can use this to examine its dilution with water from other sources. First, we define the end member to be Atlantic Water transported in the NCC and NwAC as this has been shown to be the dominant transport pathway of RP-^{236}U from the Atlantic into the Arctic (Wefing et al., 2021). Other waters (Pacific Water and freshwater including river runoff, sea ice and glacier melt water) only contain a GF signal, so their RP-^{236}U concentrations are considered to be negligible. The RP contribution of ^{236}U in Atlantic Water ($^{236}U_{RP\text{-}AW}$) is a time-dependent value and can be derived from the ^{236}U discharges from SF and LH (see supporting information; Christl et al., 2015; Casacuberta et al., 2018; Castrillejo et al., 2020), and assumptions on mixing in the North Sea and transport northwards to the Arctic, to derive Arctic input functions for NCC and NwAC (Casacuberta et al., 2018; Wefing et al., 2021). The uncertainty of $^{236}U_{RP\text{-}AW}$ can also be estimated from uncertainties of the shell record of ^{236}U/^{238}U ratios near SF and LH, and marine mixing pattern of SF branch water, LH branch water and GF (Casacuberta et al., 2018; Castrillejo et al., 2020). As shown in Fig. S1, the temporal evolutions of $^{236}U_{RP\text{-}AW}$ in both NCC (carrying tracer signal to PSW) and NwAC (carrying tracer signal to AAW) branch waters demonstrate monotonous decreasing trend over the period of 1976–2016. This means that Atlantic Water fraction contained in each sample with known RP-^{236}U concentration is only dependent on the endmember value of $^{236}U_{RP\text{-}AW}$, i.e., the source year of RP-^{236}U in the Atlantic Water (Fig. 3). Consequently, with known Atlantic Water fraction, the transit time of Atlantic Water from the entrance of Arctic Ocean to the study location can be obtained.

4.2.2. Source year estimation based on N:P-derived Atlantic Water fraction

In this study, we use nitrate and phosphate concentrations (Table S1) to estimate the Atlantic Water fraction according to Eqs. (9)–(13) (Dodd et al., 2012) thus to constrain its source year (black and grey lines in Fig. 3). The uncertainty for Atlantic Water fraction estimation with this method was approximately 10% (Dodd et al., 2012).

$$f_{AW} + f_{PW} + f_{FW} = 1 \quad (9)$$

$$f_{AW}P_{AW} + f_{FW}P_{AW} + f_{PW}P_{PW} = P_S \quad (10)$$

$$f_{AW}S_{AW} + f_{PW}S_{PW} + f_{FW}S_{FW} = S_S \quad (11)$$

where P_{AW} and P_{PW} are phosphate concentrations in Atlantic Water and Pacific Water; f_{AW}, f_{PW} and f_{FW} are Atlantic Water fraction, Pacific Water fraction and freshwater fraction in the sample collected (2018); S_{AW}, S_{PW}, S_{FW} and S_s are salinity in Atlantic Water, Pacific Water, freshwater and seawater samples, respectively. Here we assume P_{FW} is equal to P_{AW}. The calculated fractions of Atlantic Water in each sample are summarized in Table S1. In addition, phosphate concentrations for Atlantic Water and Pacific Water are based on the following equations:

$$P_{AW} = M_{AW}N + C_{AW} \quad (12)$$

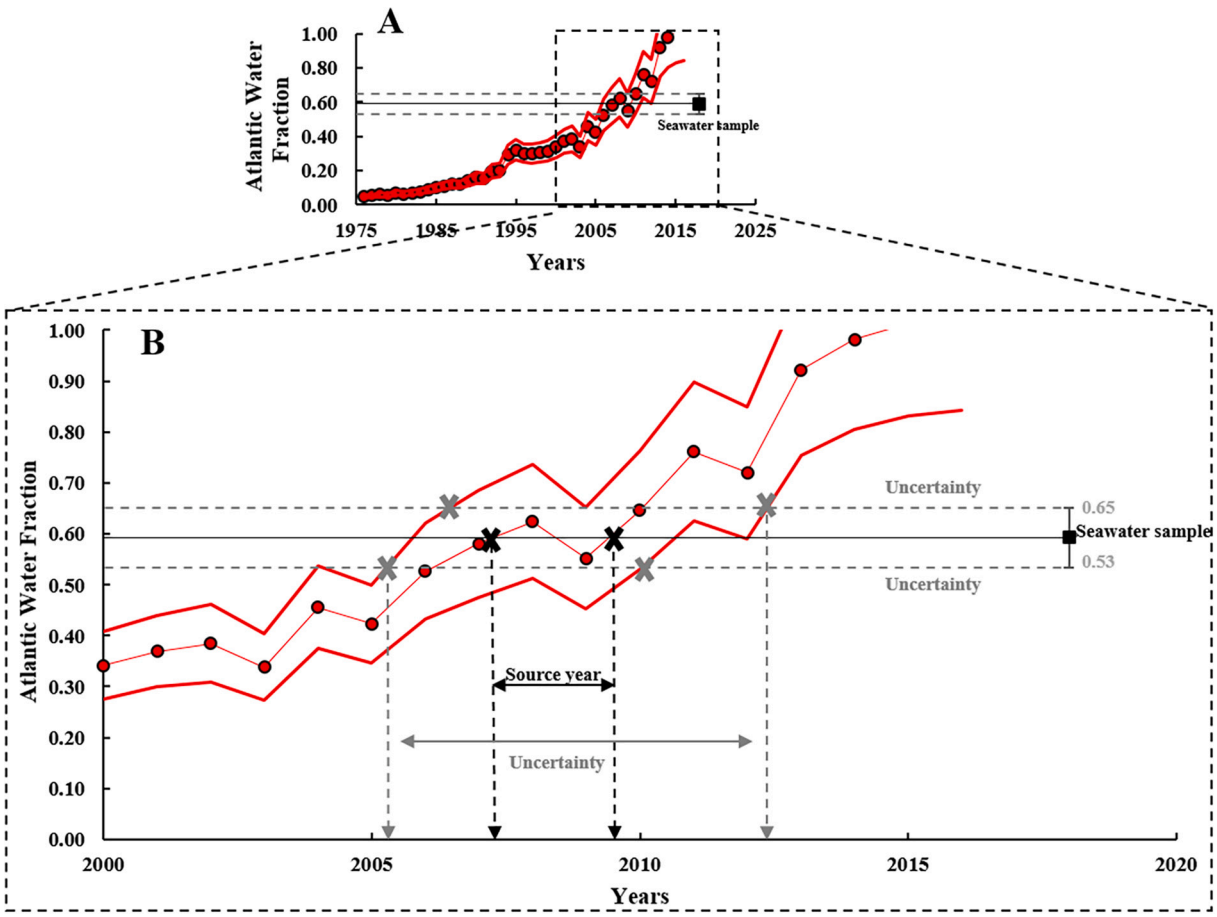

Fig. 3. An example of the fraction estimation of Atlantic Water (red dots and thin red line) with uncertainty (thick red lines) (A) and the detailed change during 2000–2020 (B). The estimation of Atlantic Water fraction for a sample with known RP-^{236}U concentration is only dependent on the end member value of $^{236}U_{RP\text{-}AW}$ which is time-depend following the NCC or NwAC input function (as shown Fig. S1). (For interpretation of the references to colour in this figure legend, the reader is referred to the web version of this article.)

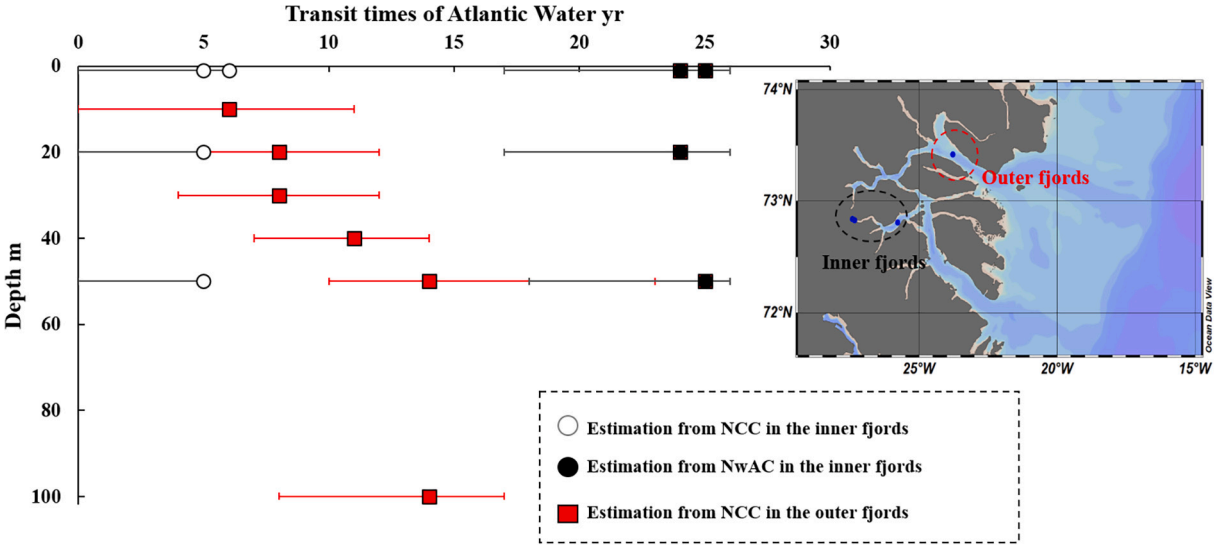

Fig. 4. Estimates of Atlantic Water transit times in the fjords based on the input functions of Norwegian Coastal Current (NCC) and Norwegian Atlantic Current (NwAC). For Polar Surface Water (PSW) in the inner fjords, transit times are estimated with both the NCC $^{236}U_{RP\text{-}AW}$ input function (open circles) and the NwAC $^{236}U_{RP\text{-}AW}$ input function (black circles). For PSW in the outer fjords transit times are estimated with the NCC $^{236}U_{RP\text{-}AW}$ input function (red squares). (For interpretation of the references to colour in this figure legend, the reader is referred to the web version of this article.)

$$P_{PW} = M_{PW}N + C_{PW} \quad (13)$$

where N is nitrate concentration in the seawater samples; M_{AW} (M_{PW}) and C_{AW} (C_{PW}) are the slope and intercept of Atlantic Water (Pacific Water) N:P relationship.

Based on the end member values in NCC branch water, the source years of Atlantic Water in PSW (upper 100 m) in the East Greenland fjords are estimated between 2004 and 2012 (uncertainties of source years: 1995–2018), suggesting that the transit times from the entrance of the Arctic Ocean are 0 years (ranging from 0 to 6 years considering uncertainties) in the inner fjords and 6–14 years (ranging from 0 to 23 years considering uncertainties) in the outer fjords (Fig. 4 open circle and red square symbols). Compared with previous results (12–17 years, Wefing et al., 2021) in polar waters on the Greenland shelf estimated from ^{129}I and ^{236}U, our results in the PSW of the fjords show a wider range. It is worth noting that the estimated transit times in the inner fjords seem not reasonable, which might be due to the impact of upwelling of AAW (see detailed explanation in Section 4.3). For the outer fjords, transit times of Atlantic Water increase with depths, which may be related to different transport pathways (Fig. 4).

4.3. The impact of upwelling on transit time estimation of Atlantic Water

While the majority of estimations of Atlantic Water transit times in the fjords are reasonable, there are however exceptions. The four samples (open circle in Fig. 4) from the inner parts of the fjords have unrealistically short transit times ($\leq$ 6 years). Comparison with other samples at the same depth reveals that these samples have higher fractions of Atlantic Water (e.g. 93% at inner fjord vs. 63% at outer fjord at 50 m depth) and freshwater (e.g. 7% at inner fjord vs. 5% at outer fjord at 50 m depth) but lower Pacific Water contributions (e.g. -1% at inner fjord vs. 32% at outer fjord at 50 m depth) (Fig. 5A-C). This might be

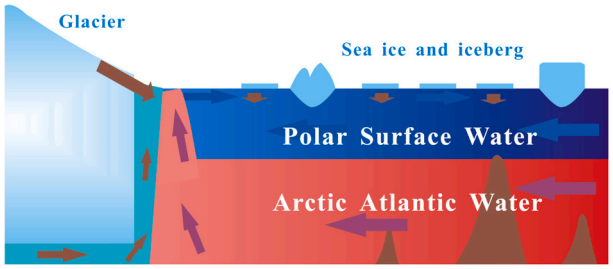

Fig. 6. Schematic of water column stratification in East Greenland fjords.

because these waters are influenced by subglacial discharge, which causes upwelling at the terminus and entrains AAW to the surface, restricting the lateral extent of polar waters (Fig. 6). This is also reflected by lower RP-^{236}U concentrations in these samples compared to those from the remaining part of the fjord (e.g., 14.4 ± 1.6 × 10^6 atom/L in the inner fjord vs. 27.6 ± 3.6 × 10^6 atom/L in the outer fjord at 100 m depth), revealing that the RP ^{236}U signal is diluted by upwelling entrained Greenlandic meltwater (no RP signal) and older AAW (low RP signal) (Fig. 5B). The entrainment of AAW from upwelling and lack of surface Atlantic Water contribution implies that transit time estimate for samples in the inner fjords should be further constrained by taking into account fjord circulation and re-considering the use of the appropriate input function. In the inner parts of the fjords where glacial upwelling entrains AAW to the surface and the influence of Pacific Water (PW) is limited, and the NwAC $^{236}U_{RP\text{-}AW}$ input function is more appropriate to use.

AAW on the East Greenland Shelf with (temperature 1.17–1.54 °C and salinity 34.71–34.89 in Fig. 2A-B), has its origins in the NwAC (Wefing et al., 2019; Wefing et al., 2021), which has its own RP ^{236}U input function at the entrance of Arctic (74°N, 19°E) (Fig. S2, supporting

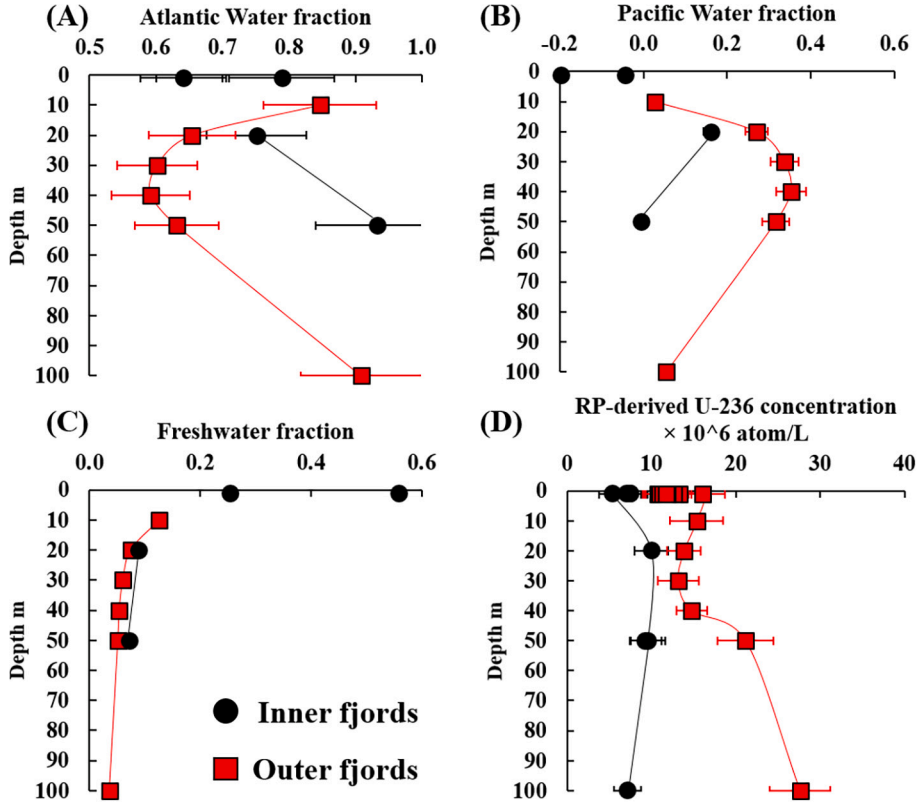

Fig. 5. The fractions of Atlantic Water (A), Pacific Water (B) and freshwater (C) in the profiles of the inner fjords (black circles) and the outer fjords (red squares) estimated from nitrate, phosphate and salinity and RP-derived ^{236}U concentrations in the profile of the inner fjords (black circles) and the outer fjords (red squares) (D). (For interpretation of the references to colour in this figure legend, the reader is referred to the web version of this article.)

information). Replacing the NCC input function with NwAC for the surface water samples in the inner fjord, results in transit times on the order of 24–25 years (ranging from 17 to 27 years considering uncertainties) (Fig. 4, black dot). Our estimations are slightly higher than the transit times for the AAW (16–23 years) on the western Fram Strait (Wefing et al., 2019). This is reasonable as it takes extra time for Atlantic Water exiting from western Fram Strait to reach East Greenland fjords. In this study, we assume the purely advective transport in the Arctic Ocean due to the strong stratification and vertical mixing was considered limited. Therefore, single NwAC input function can be considered in the AAW. In addition, the Returning Atlantic Current (RAC) can reach Northeast Greenland fjords through the Fram Strait without entering the Arctic Ocean (Schaffer et al., 2017), implying possible appearance of younger Atlantic Water in this region. However, it is not clear whether RAC is present in the study area, as so far no report has verified the contribution of RAC in East Greenland fjords. Therefore, contribution of RAC fraction (if any) was not considered in our Atlantic Water transit time estimation.

4.4. The limitations and uncertainties of the ^{233}U-^{236}U tracer approach

Although the approach provides plausible transit times which are comparable with published data, there are still limitations and uncertainties associated with these estimates. The proposed ^{233}U-^{236}U tracer approach is based on the assumption of purely advective transport of input function signals to the study region. One can question the validity of this assumption, but the observed widespread stratification in the region hints to limited deep vertical mixing in these waters sampled. The nutrient based approach used here to isolate the Atlantic Water fraction also has considerable limitations. It assumes the preferential loss of nitrate (to denitfircation), relative to phosphate, only occurs on shelf waters influenced by the Pacific inflow (Jones et al., 1998). However, there is clear evidence that Siberian shelf waters can also contribute (Alkire et al., 2015; Bauch et al., 2011) and that there may be considerable errors in the estimates of Pacific water in the central Arctic (Alkire et al., 2015; Whitmore et al., 2020). Similarly it is unclear if interactions with Greenland shelf sediments during passage over fjord sills can generate an artificial Pacific Water signal. With this in mind it would certainly be relevant to expand on this explorative study to include greater coverage of additional tracers for water fractionation and better geographical coverage of sampling to map source waters. Additional chemical tracers (such as ^{99}Tc, ^{137}Cs and ^{129}I) could also add to further validate this new ^{233}U-^{236}U tracer approach.

We also acknowledge that part of the relatively high uncertainty (up to 40%) in the current transit time estimation can be due to the ultra-low levels of ^{233}U in environmental samples and limitation in achieving high precision in $^{236}U/^{233}U$ (currently at level of 30%) measurement by AMS. This could in part be rectified by using larger sample volume to achieve increased detection efficiency in the AMS measurement. Finally the approach also hinges on the validity of the input function estimates and mixing of SF and LH branch water. Nevertheless, our results (6–14 years) in the outer fjords agree well with previous study, indicating success in our exploration to use ^{233}U and ^{236}U to estimate transit times of Atlantic Water in East Greenland fjords. Therefore, the paired anthropogenic uranium (^{233}U and ^{236}U) tracer approach, combining with salinity and nutrients (nitrate and phosphate), may hold promise as a technique to isolate RP ^{236}U and estimate Atlantic water transit times in Arctic and subpolar regions.

5. Conclusions and perspectives

In this work, we developed a new approach based on paired tracer ^{233}U-^{236}U and nutrient data for estimating Atlantic Water transit time in the Arctic Ocean. ^{233}U was used to isolate reprocessing contribution of ^{236}U to exclusively trace the Atlantic Water, and nitrate and phosphate were measured to constrain the Atlantic Water fraction, thereby to derive the transit time based on the time-dependent variation of ^{236}U in the Atlantic Water end member. The significantly distinct source term distribution of ^{236}U in PSW (63% from RP contributions) and in AAW (74% from GF contributions) makes the ^{233}U-^{236}U signal very useful fingerprint to distinguish these two water bodies in the Arctic region.

Based on the estimation with the ^{233}U-^{236}U approach, the transit time of Atlantic Water in outer East Greenland fjords is 6–14 years, while that in inner East Greenland fjords is 24–25 years. These estimates were in good agreement with earlier studies in the northeastern Greenland coast (Wefing et al., 2019). The estimates in this work using the ^{233}U-^{236}U tracer pair offer a first approximation of transit times which can be constrained in the future by further sampling with higher spatial resolution and comparison with ocean circulation model results.

The transit times estimated in this work provide an indication of the time lag that can be expected between alterations in the waters entering the Arctic to a subsequent effect on the water leaving the Arctic Ocean on the East Greenland shelf. As transit times for Atlantic Water are on the order of 24–25 years any changes in the Atlantic waters flowing into the Arctic, can be expect to materialize in outflowing waters approximately 25 years later. Although it should also be noted that variability in ocean circulation conditions directly upstream of the Greenland shelf, in the central Arctic, likely have a greater influence on water properties in the region. Although this extrapolation may be speculative and further investigations are needed, these measurements provide an indication of the potential timescale of propagation of a signal from the Atlantic to the Greenland shelf.

Declaration of Competing Interest

The authors declare that they have no known competing financial interests or personal relationships that could have appeared to influence the work reported in this paper.

Acknowledgements

We acknowledge the financial support of the Independent Research Fund Denmark (9040-00266B). Part of the AMS measurements at VERA were supported by the RADIATE project from the EU Research and Innovation programme HORIZON 2020 under grant agreement No 824096, proposal No. 21002394-ST. L.M. was funded by research programme VENI with project number 016.Veni.192.150, which is financed by the Dutch Research Council (NWO). We also thank the captain and crews of the Royal Danish Naval vessel HMDS Lauge Koch for their support with sampling at Northeast Greenland.

Appendix A. Supplementary data

Supplementary data to this article can be found online at https://doi.org/10.1016/j.chemgeo.2022.121007.

References

Aagaard, K., Carmack, E.C., 1989. The role of sea ice and other fresh water in the Arctic circulation. J. Geophys. Res. Ocean 94 (10), 14485–14498. https://doi.org/10.1029/JC094iC10p14485.

Alkire, M.B., Morison, J., Andersen, R., 2015. Variability in the meteoric water, sea-ice melt, and Pacific Water contributions to the Central Arctic Ocean, 2000-2014. J. Geophys. Res. Oceans 120 (3), 1573–1598. https://doi.org/10.1002/2014JC010023.

Andersson, P.S., Wasserburg, G.J., Chen, J.H., Papanastassiou, D.A., Ingri, J., 1995. ^{238}U-^{234}U and ^{232}Th-^{230}Th in the Baltic Sea and in river water. Earth Planet. Sci. Lett. 130, 217–234. https://doi.org/10.1016/0012-821X(94)00262-W.

Bauch, D., van der Loeff, M.R., Andersen, N., Torres-Valdes, S., Bakker, K., Abrahamsen, E.P., 2011. Origin of freshwater and polynya water in the Arctic Ocean halocline in summer 2007. Prog. Oceanogr. 91 (4), 482–495. https://doi.org/10.1016/j.pocean.2011.07.017.

Beszczynska-Möller, A., Woodgate, R.A., Lee, C., Melling, H., Karcher, M., 2011. A synthesis of exchanges through the main oceanic gateways to the Arctic Ocean. Oceanography 24 (3), 82–99. https://doi.org/10.5670/oceanog.2011.59.

BIPM, IEC, IFCC, ISO, IUPAC, IUPAP, OIML, 2008. Evaluation of measurement data—Guide to the expression of uncertainty in measurement. Jt. Comm. Guid. Metrol. 100, 1–116.
Casacuberta, N., Christl, M., Lachner, J., van der Loeff, M.R., Masqué, P., Synal, H.-A., 2014. A first transect of ^{236}U in the North Atlantic Ocean. Geochim. Cosmochim. Acta 133, 34–46. https://doi.org/10.1016/j.gca.2014.02.012.
Casacuberta, N., Masqué, P., Henderson, G., Rutgers van der Loeff, M., Bauch, D., Vockenhuber, C., Daraoui, A., Walther, C., Synal, H.-A., Christl, M., 2016. First ^{236}U data from the Arctic Ocean and use of ^{236}U/^{238}U and ^{129}I/^{236}U as a new dual tracer. Earth Planet. Sci. Lett. 440, 127–134. https://doi.org/10.1016/j.epsl.2016.02.020.
Casacuberta, N., Christl, M., Vockenhuber, C., Wefing, A.-M., Wacker, L., Masqué, P., Synal, H.-A., van der Loeff, M.R., 2018. Tracing the three Atlantic branches entering the Arctic Ocean with ^{129}I and ^{236}U. J. Geophys. Res. Oceans 123, 6909–6921. https://doi.org/10.1029/2018JC014168.
Castrillejo, M., Witbaard, R., Casacuberta, N., Richardson, C.A., Dekker, R., Synal, H.-A., Christl, M., 2020. Unravelling 5 decades of anthropogenic ^{236}U discharge from nuclear reprocessing plants. Sci. Total Environ. 717, 137094. https://doi.org/10.1016/j.scitotenv.2020.137094 (2020).
Christl, M., Lachner, J., Vockenhuber, C., Lechtenfeld, O., Stimac, I., van der Loeff, M.R., Synal, H.-A., 2012. A depth profile of uranium-236 in the Atlantic Ocean. Geochim. Cosmochim. Acta 77, 98–107. https://doi.org/10.1016/j.gca.2011.11.009.
Christl, M., Casacuberta, N., Vockenhuber, C., Elsässer, C., Bailly du Bois, P., Herrmann, J., Synal, H.A., 2015. Reconstruction of the ^{236}U input function for the Northeast Atlantic Ocean: Implications for ^{129}I/^{236}U and ^{236}U/^{238}U-based tracer ages. J. Geophys. Res. Oceans 120, 7282–7299. https://doi.org/10.1002/2015JC011116.
Christl, M., Casacuberta, N., Lachner, J., Herrmann, J., Synal, H.-A., 2017. Anthropogenic ^{236}U in the North Sea—a closer look into a source region. Environ. Sci. Technol. 51, 12146–12153. https://doi.org/10.1021/acs.est.7b03168.
Dahlgaard, H., 1995. Transfer of European coastal pollution to the arctic: Radioactive tracers. Mar. Pollut. Bull. 31, 3–7. https://doi.org/10.1016/0025-326X(95)00003-6.
Dodd, P.A., Rabe, B., Hansen, E., Falck, E., Mackensen, A., Rohling, E., Stedmon, C.A., Kristiansen, S., 2012. The freshwater composition of the Fram Strait outflow derived from a decade of tracer measurements. J. Geophys. Res. 117, C11005. https://doi.org/10.1029/2012JC008011.
Dunk, R.M., Mills, R.A., Jenkins, W.J., 2002. A reevaluation of the oceanic uranium budget for the Holocene. Chem. Geol. 190, 45–67. https://doi.org/10.1016/S0009-2541(02)00110-9.
Eigl, R., Srncik, M., Steier, P., Wallner, G., 2013. ^{236}U/^{238}U and ^{240}Pu/^{239}Pu isotopic ratios in small (2*L*) sea and river water samples. J. Environ. Radioact. 116, 54–58. https://doi.org/10.1016/j.jenvrad.2012.09.013.
Fine, R.A., 2011. Observations of CFCs and SF6 as Ocean tracers. Annu. Rev. Mar. Sci. 3, 173–195. https://doi.org/10.1146/annurev.marine.010908.163933.
Gjelstrup, C.V.B., Sejr, M.K., Christiansen, J.S., Dodd, P.A., Granskog, M.A., Koch, B., Møller, E.F., de Steur, L., Winding, M.S., Stedmon, C.A., 2022. Warm Meets Fresh: Decadal Changes in Water Properties on the Northeast Greenland Shelf (in review).
Hain, K., Steier, P., Froehlich, M.B., Golser, R., Hou, X., Lachner, J., Qiao, J., Quinto, F., Sakaguchi, A., 2020. ^{233}U/^{236}U signature allows to distinguish environmental emissions of civil nuclear industry from weapons fallout. Nat. Commun. 11 https://doi.org/10.1038/s41467-020-15008-2.
Hansen, H.P., Koroleff, F., 1999. Determination of nutrients. In: Grasshoff, K., Kremling, K., Ehrhardt, M. (Eds.), Methods of Seawater Analysis, 3rd ed. Wiley-VCH, Weinheim, Germany, pp. 159–228. https://doi.org/10.1002/9783527613984.ch10.
HELCOM MORS Discharge database [WWW Document]. n.d. https://helcom.fi/baltic-sea-trends/data-maps/databases/ (accessed 5.20.2020).
Ionita, M., Scholz, P., Lohmann, G., Dima, M., Prange, M., 2016. Linkages between atmospheric blocking, sea ice export through Fram Strait and the Atlantic Meridional Overturning Circulation. Sci. Rep. 6 (1), 32881. https://doi.org/10.1038/srep32881.
Jones, E.P., Anderson, L.G., Swift, J.H., 1998. Distribution of Atlantic and Pacific waters in the upper Arctic Ocean: implications for circulation. Geophys. Res. Lett. 25, 765–768. https://doi.org/10.1029/98GL00464.
Klimkhammer, G.P., Palmer, M.R., 1991. Uranium in the oceans: where it goes and why. Geochim. Cosmochim. Acta 55, 1799–1806.
Lin, M., Qiao, J.X., Hou, X.L., Dellwig, O., Steier, P., Hain, K., Golser, R., Zhu, L.C., 2021a. 70-Year anthropogenic uranium imprints of nuclear activities in Baltic Sea sediments. Environ. Sci. Technol. 55 (13), 8918–8927. https://doi.org/10.1021/acs.est.1c02136.
Lin, M., Qiao, J.X., Hou, X.L., Golser, R., Hain, K., Steier, P., 2021b. On the quality control for the determination of ultratrace-level ^{236}U and ^{233}U in environmental samples by accelerator mass spectrometry. Anal. Chem. 93, 3362–3369. https://doi.org/10.1021/acs.analchem.0c03623.
Polyakov, I.V., Pnyushkov, A.V., Alkire, M.B., Ashik, I.M., Baumann, T.M., Carmack, E.C., Goszczko, I., Guthrie, J., Ivanov, V.V., Kanzow, T., Krishfield, R., Kwok, R., Sundfjord, A., Morison, J., Rember, R., Yulin, A., 2017. Greater role for Atlantic inflows on sea ice loss in the Eurasian Basin of the Arctic Ocean. Science 356 (6335), 285–291. https://doi.org/10.1126/science.aai8204.
Qiao, J.X., Ransby, D., Steier, P., 2022. Deciphering anthropogenic uranium sources in the equatorial northwest Pacific margin. Sci. Total Environ. 806, 150482. https://doi.org/10.1016/j.scitotenv.2021.150482.
Qiao, J.X., Xu, Y.H, 2018. Direct measurement of uranium in seawater by inductively coupled plasma mass spectrometry. Talanta 183, 18–23. https://doi.org/10.1016/j.talanta.2018.02.045.
Qiao, J.X., Hou, X.L., Steier, P., Nielsen, S., Golser, R., 2015. Method for ^{236}U determination in seawater using flow injection extraction chromatography and accelerator mass spectrometry. Anal. Chem. 87, 7411–7417. https://doi.org/10.1021/acs.analchem.5b01608.
Qiao, J.X., Hain, K., Steier, P., 2020. First dataset of ^{236}U and ^{233}U around the Greenland coast: A 5-year snapshot (2012–2016). Chemosphere 257, 127185. https://doi.org/10.1016/j.chemosphere.2020.127185.
Rahmstorf, S., 2002. Ocean circulation and climate during the past 120,000 years. Nature 419, 207–214. https://doi.org/10.1038/nature01090.
Rudels, B., 2009. Arctic Ocean circulation. In: Encyclopedia of Ocean Sciences, pp. 211–225. https://doi.org/10.1016/B978-012374473-9.00601-9.
Rudels, B., Jones, E.P., Schauer, U., Eriksson, P., 2004. Atlantic sources of the Arctic Ocean surface and halocline waters. Polar Res. 23 (2), 181–208. https://doi.org/10.3402/polar.v23i2.6278.
Rutgers van der Loeff, M.M., Geibert, W., 2008. U-and Th-series nuclides as tracers of particle dynamics, scavenging and biogeochemical cycles in the Oceans. In: Krishnaswami, S., Cochran, J.K. (Eds.), Radioactivity in the Environment, 13, pp. 227–268. https://doi.org/10.1016/S1569-4860(07)00007-1.
Sakaguchi, A., Kawai, K., Steier, P., Quinto, F., Mino, K., Tomita, J., Hoshi, M., Whitehead, N., Yamamoto, M., 2009. First results on ^{236}U levels in global fallout. Sci. Total Environ. 407, 4238–4242. https://doi.org/10.1016/j.scitotenv.2009.01.058.
Sakaguchi, A., Kadokura, A., Steier, P., Takahashi, Y., Shizuma, K., Hoshi, M., Nakakuki, T., Yamamoto, M., 2012. Uranium-236 as a new oceanic tracer: a first depth profile in the Japan Sea and comparison with caesium-137. Earth Planet. Sci. Lett. 333, 165–170. https://doi.org/10.1016/j.epsl.2012.04.004.
Sakaguchi, A., Nomura, T., Steier, P., Golser, R., Sasaki, K., Watanabe, T., Nakakuki, T., Takahashi, Y., Yamano, H., 2016. Temporal and vertical distributions of anthropogenic ^{236}U in the Japan Sea using a coral core and seawater samples. J. Geophys. Res. Oceans 121, 4–13. https://doi.org/10.1002/2015JC011109.
Schaffer, J., von Appen, W.-J., Dodd, P.A., Hofstede, C., Mayer, C., de Steur, L., Kanzow, T., 2017. Warm water pathways toward Nioghalvfjerdsfjorden Glacier, Northeast Greenland. J. Geophys. Res. Oceans 122 (5), 4004–4020. https://doi.org/10.1002/2016JC012462.
Schaffer, J., Kanzow, T., von Appen, W.-J., von Albedyll, L., Arndt, J.E., Roberts, D.H., 2020. Bathymetry constrains ocean heat supply to Greenland's largest glacier tongue. Nat. Geosci. 13, 227–231. https://doi.org/10.1038/s41561-019-0529-x.
Schwehr, K.A., Scantschi, P.H., Elmore, D., 2005. The dissolved organic iodine species of the isotopic ratio of 129I/127I: a novel tool for tracing terrestrial organic carbon in the estuarine surface waters of Galveston Bay, Texas. Limnol. Oceanogr. Methods 3, 326–337. https://doi.org/10.4319/lom.2005.3.326.
Sejr, M.K., Stedmon, C.A., Bendtsen, J., Abermann, J., Juul-Pedersen, T., Mortensen, J., Rysgaard, S., 2017. Evidence of local and regional freshening of Northeast Greenland coastal waters. Sci. Rep. 7, 13183. https://doi.org/10.1038/s41598-017-10610-9.
Serreze, M.C., Barrett, A.P., Slater, A.G., Woodgate, R.A., Aagaard, K., Lammers, R.B., Steele, M., Moritz, R., Meredith, M., Lee, C.M., 2006. The large-scale freshwater cycle of the Arctic. J. Geophys. Res. 111, C11010. https://doi.org/10.1029/2005JC003424.
Skagseth, Ø., Eldevik, T., Årthun, M., Asbjørnsen, H., Lien, V.S., Smedsrud, L.H., 2020. Reduced efficiency of the Barents Sea cooling machine. Nat. Clim. Chang. 10, 661–666. https://doi.org/10.1038/s41558-020-0772-6.
Smith, J.N., McLaughlin, F.A., Smethie, W.M., Moran, S.B., Lepore, K., 2011. Iodine-129, ^{137}Cs, and CFC-11 tracer transit time distributions in the Arctic Ocean. J. Geophys. Res. 116 (C04024), 2011. https://doi.org/10.1029/2010JC006471.
Steier, P., Bichler, M., Keith Fifield, L., Golser, R., Kutschera, W., Priller, A., Quinto, F., Richter, S., Srncik, M., Terrasi, P., Wacker, L., Wallner, A., Wallner, G., Wilcken, K. M., Maria Wild, E., 2008. Natural and anthropogenic ^{236}U in environmental samples. Nucl. Inst. Methods Phys. Res. B 266, 2246–2250. https://doi.org/10.1016/j.nimb.2008.03.002.
Steier, P., Dellinger, F., Forstner, O., Golser, R., Knie, K., Kutschera, W., Priller, A., Quinto, F., Srncik, M., Terrasi, F., Vockenhuber, C., Wallner, A., Wallner, G., Wild, E. M., 2010. Analysis and application of heavy isotopes in the environment. Nucl. Inst. Methods Phys. Res. B 268 (7–8), 1045–1049. https://doi.org/10.1016/j.nimb.2009.10.094.
Steier, P., Hain, K., Klötzli, U., Lachner, J., Priller, A., Winkler, S., Golser, R., 2019. The Actinide Beamline at VERA. Nucl. Instrum. Methods Phys. Res. Sect. B Beam Interact. Mater. At. 458, 82–89. https://doi.org/10.1016/j.nimb.2019.07.031.
Tsubouchi, T., Våge, K., Hansen, B., Larsen, K.M.H., Østerhus, S., Johnson, C., Jonsson, S., Valdimarsson, H., 2021. Increased ocean heat transport into the Nordic Seas and Arctic Ocean over the period 1993–2016. Nat. Clim. Chang. 11, 21–26. https://doi.org/10.1038/s41558-020-00941-3.
Tsungogai, S., Henmi, T., 1971. Iodine in the surface water of the Ocean. J. Oceanogr. Soc. Jpn. 27, 67–72.
Villa-Alfageme, M., Chamizo, E., Kenna, T.C., López-Lora, M., Casacuberta, N., Chang, C., Masqué, P., Christl, M., 2019. Distribution of ^{236}U in the U.S. GEOTRACES Eastern Pacific Zonal Transect and its use as a water mass tracer. Chem. Geol. 517, 44–57. https://doi.org/10.1016/j.chemgeo.2019.04.003.
Wang, Q., 2021. Stronger variability in the Arctic Ocean induced by sea ice decline in a warming climate: Freshwater storage, dynamic sea level and surface circulation. J. Geophys. Res. Oceans 126. https://doi.org/10.1029/2020JC016886 e2020JC016886.

Wefing, A.-M., Christl, M., Vockenhuber, C., Rutgers van der Loeff, M., Casacuberta, N., 2019. Tracing Atlantic waters using ^{129}I and ^{236}U in the Fram Strait in 2016. J. Geophys. Res. Oceans 124, 882–896. https://doi.org/10.1029/2018JC014399.

Wefing, A.-M., Casacuberta, N., Christl, M., Gruber, N., Smith, J.N., 2021. Circulation timescales of Atlantic Water in the Arctic Ocean determined from anthropogenic radionuclides. Ocean Sci. 17, 111–129. https://doi.org/10.5194/os-17-111-2021.

Whitmore, L.M., Pasqualini, A., Newton, R., Shiller, A.M., 2020. Gallium: a new tracer of Pacific Water in the Arctic Ocean. J. Geophys. Res. Oceans 125. https://doi.org/10.1029/2019JC015842 e2019JC015842.